

Electrochemically deposited Cu₂O cubic particles on boron doped diamond substrate as efficient photocathode for solar hydrogen generation

Christos K. Mavrokefalos¹, Maksudul Hasan^{*1,2}, James F. Rohan², Richard G. Compton³ and John S. Foord^{*1}

¹Department of Chemistry, Chemistry Research Laboratory, University of Oxford, Mansfield Road, Oxford, OX1 3TA, England, UK

²Tyndall National Institute, University College Cork, Lee Maltings, Cork, Ireland

³Department of Chemistry, Physical and Theoretical Chemistry Laboratory, University of Oxford, South Parks Road, Oxford, OX1 3QZ, England, UK

*Corresponding author: E-mail: maksudul.hasan@chem.ox.ac.uk;
john.foord@chem.ox.ac.uk Phone: +44 01865 275967-75630 Fax: +44 01865 275410

Abstract: Herein, we report a novel photocathode for the water splitting reaction. The electrochemical deposition of Cu₂O particles on boron doped diamond (BDD) electrodes and the subsequent decoration with NiO nanoparticles by a dip coating method to act as co-catalyst for hydrogen evolution reaction is described. The morphology analysis by scanning electron microscope (SEM) revealed that Cu₂O particles are cubic and decorated sporadically with NiO nanoparticles. X-ray photoelectron spectroscopy (XPS) confirmed the electronic interaction at the interface between Cu₂O and NiO through a binding energy shift of the main Cu 2p peak. The photoelectrochemical (PEC) performance of NiO-Cu₂O/BDD showed a much higher current density (-0.33 mA/cm²) and photoconversion efficiency (0.28%) compared to the unmodified Cu₂O/BDD electrode, which are only -0.12 mA/cm² and 0.06%, respectively. The enhancement in PEC performance is attributable to the synergy of NiO as an electron conduction mediator leading to the enhanced charge separation and transfer to the reaction interface for hydrogen evolution as evidenced by electrochemical impedance spectroscopy (EIS) and charge carrier density calculation. Stability tests showed that the NiO nanoparticles loading content on Cu₂O surface is a crucial parameter in this regard.

Keywords: Diamond, Copper Oxide, Photocatalysts, Solar Fuels, Water Splitting, Hydrogen Energy.

1. Introduction

One of the major challenges facing our today's society is the climate change due to massive fossil fuels consumption as a primary energy source. The depletion of fossil fuels and continuous increase in our daily energy demands have urged for the development of renewable energy sources. The solar fuels production by artificial photosynthesis is an attractive and sustainable solution to address the challenges of climate change and fossil fuel depletion. Solar water splitting into hydrogen and oxygen is a promising means of storing solar energy in the chemical bonds, usually hydrogen molecules, since both water and sunlight are abundant [1-5]. Hydrogen is widely regarded as a key energy solution for the 21st century due to its high mass energy density and being environmentally benign [6]. Collection, conversion and storage of solar energy are three processes that can be integrated into a single photoelectrochemical (PEC) cell within which the solar energy can be converted into stored chemical energy within the H-H bonds as hydrogen gas molecules [7-9]. Hence, water splitting in a PEC cell has attracted an increasing research effort in both academia and industry [5, 10-12].

In principle, photocatalysts consist of visible light absorption semiconductor materials as the redox mediators for hydrogen and oxygen evolution reactions. The semiconductor materials must have a sufficiently narrow direct bandgap in order to absorb a large portion of the solar spectrum, good electrical conductivity for the photogenerated charge carriers and stability in an aqueous environment [13]. Copper (I) oxide (Cu_2O), is a naturally occurring p-type semiconductor with a direct band gap of 2.17 eV and is, therefore, an attractive photocathode material. Its direct band gap permits efficient visible light absorption [14-19] while also possessing a necessary conduction band at around 0.7 V negative of the hydrogen evolution potential [16,19]. However, one of the main drawbacks of Cu_2O is its instability due to self-photo-corrosion in contact of water under illumination [20]. Various methods for the synthesis of photoactive Cu_2O have been reported previously, including thermal relaxation [21], holographic lithography [22], sputtering [23], thermal evaporation [24], and electrochemical synthesis [25-30]. The obstacle of self-photo-corrosion of Cu_2O could be overcome if Cu_2O were combined with a suitable co-catalyst to assist the rapid separation and transportation of photogenerated electrons to the reaction interface for protons reduction [31,32], and thus, the stability of Cu_2O can be improved in aqueous solutions [18,33-35]. The photo-response of semiconductors was previously improved by using carbon coating [36]

nickel hydroxide [37-39] and nickel oxide [40-45] as a protecting layer for solar hydrogen generation.

On the other hand, one very promising candidate as a catalyst support for sustainable technologies is boron-doped diamond (BDD). As reported in previous work [46] BDD possesses a wide potential window, low background current, resistance to fouling, resistance to electrocorrosion, very stable chemical terminations [47,48] and is available at a low economic cost when grown by chemical vapour deposition (CVD). Hence, it can support the charge separation within the semiconductor and in general facilitate the photocatalytic activities.

In this work, we report the electrochemical modification of BDD electrode with Cu₂O-NiO particles. The method involves the electrodeposition of Cu₂O cubic particles on BDD from surfactant free “green” electrolyte followed by coating of NiO nanoparticles by dip coating containing an alcoholic solution of nickel acetate as precursor. The electrochemical experimental data showed that a co-catalyst effect of NiO nanoparticles leads to a higher photocurrent densities and stabilities by comparison with Cu₂O photocatalyst alone. In order to understand the correlation between the morphological, particle dispersion and photoelectrochemical activities of the deposits they were characterised by high resolution scanning electron microscopy (SEM) and X-ray photoelectron spectroscopy (XPS).

2. Experimental Section

2.1 Chemical reagents

The chemical reagents copper (II) sulfate pentahydrate (CuSO₄·5H₂O), sodium hydroxide (NaOH), L-(+)-lactic acid (C₃H₆O₃), nickel (II) acetate tetrahydrate (Ni(CH₃COO)₂·4H₂O), ethanolamine (HOCH₂CH₂NH₂), 2-methoxyethanol (CH₃OCH₂CH₂OH) and sodium sulfate (Na₂SO₄) were purchased from Sigma-Aldrich and used as received without any further purification. All aqueous solutions were freshly prepared using milli-Q water (18 MΩ cm).

2.2 Equipment and experimental set-up

BDD solid wafers (Boron doping concentration >10²⁰ cm⁻³) of 10 x 10 x 0.6 mm were obtained from Element Six Co (UK). A working area of 1 cm² was exposed to the electrolyte. An Autolab PGSTAT 128N potentiostat/galvanostat was used for the electrodeposition and photoelectrochemical measurements. The data were analysed with OriginPro 8.5 software (OriginLab Ltd.). The morphology of the deposits was characterised by a FEI Helios Nanolab 600i field emission scanning electron microscope with an attached Oxford Instruments AZtech X-Max-80 energy dispersive X-ray spectroscopy unit for elemental mapping. All the

images were taken with an acceleration voltage of 20 kV and a working distance (WD) of around 4 mm. The composition of the deposits was measured by XPS using an Al K α (1486.6 eV) X-ray source. XPS data were curve fitted using CasaXPS software [49], using a Shirley background [50]. The C 1s peak was calibrated to 285 eV with the following relative sensitivity factors: C 1s (1.0), O 1s (2.93), Cu 2p (16.7) and Ni 2p (22.2). Transmission electron microscopy (TEM) was performed using a JEOL JEM-2100 at 200kV in bright field mode. Cross sections were prepared using a DualBeam focused ion beam (FIB) FEI Helios NanoLab 600i. Three protecting layers have been grown before the milling process within the DualBeam FIB, in which a 50 nm C layer followed by a 300 nm Pt layer were deposited by electron beam induced deposition and 2 μ m thick C layer with ion beam induced deposition. The lamellae were prepared and thinned down to less than 200 nm thick. The thinning at 30 kV was finished by polishing at 5 kV to reduce the ion-beam induced damage to a less than 2 nm thin layer on both sides.

2.3 Modification of BDD electrodes

Cu₂O catalyst was electrodeposited onto BDD from a freshly prepared bath of 1.5M lactic acid and 1.9M NaOH solution containing 0.2M CuSO₄·5H₂O by a galvanostatic method. The deposition current was held at -6.6 mA (vs. Ag/AgCl) for 60 sec. The Cu₂O/BDD electrode was then removed, rinsed with ultrapure water and dried with N₂ gas. The Cu₂O cubic particles on BDD electrode were modified with NiO_x by dip coating in an alcoholic solution of nickel acetate followed by annealing in air at 200°C for 3 hours. The precursor solution was made of 0.5M nickel acetate in 0.5M ethanolamine and 2-methoxyethanol. A dip coating unit was used for the adsorption of Ni⁺² ions onto Cu₂O cubic particles, which operated by a precision servo motor controlled linear stage operated at a speed of 0.35 cm/min motor. The procedure was repeated up to 20 times to achieve the optimised amount of NiO nanoparticles loading onto Cu₂O particles. Between each dip coating the electrode was dried in a pre-heated oven at 200°C for 5 min before a final annealing at this temperature for 3 hours. The number of NiO dip coating cycles for each electrode is denoted by the respective number in brackets e.g., for three repeated coatings the electrode is represented by NiO(3)-Cu₂O.

2.4 Photoelectrochemical measurement

The photoelectrochemical (PEC) measurements were performed with a 100W Xenon lamp (LCS-100 solar simulator) equipped with AM 1.5 filter and connected to an Autolab PGSTAT 128N potentiostat/galvanostat. The intensity of the light source is 1 sun (100 mW/cm²). The measurements were conducted at room temperature (24 \pm 1.0°C) using a

standard three electrode cell with a Pt counter electrode and a Ag/AgCl (1M KCl) reference electrode. The potential measured against the Ag/AgCl/saturated KCl were converted to the reversible hydrogen electrode (RHE) scale using the equation $V_{\text{RHE}} = V_{\text{Ag/AgCl(1 M KCl)}} + 0.059 \times \text{pH} + 0.22 \text{ V}$ (standard potential of Ag/AgCl/1M KCl vs. RHE). The electrolyte was an aqueous Na₂SO₄ solution (0.1M, pH 6.5). The working electrode with an electrolyte exposed area of 1 cm² was illuminated from the front side. The photoelectrochemical responses were performed using linear sweep voltammetry (LSV) at a scan rate of 10 mV/s under chopped light illumination with 5s light on/off cycles (0.2Hz). The photoelectrochemical stability of the NiO-Cu₂O/BDD electrode was evaluated by measuring the photocurrent densities under chopped light (0.2Hz) at a fixed potential of 0.05V vs. RHE. The electrochemical impedance spectroscopy (EIS) measurements were performed using the Autolab PGSTAT 128N coupled with a frequency analyser module (FRA 2) an AC amplitude of 10 mV and frequency range between 1000 kHz to 0.1 Hz. All EIS measurements were carried out at 0.05 V vs. RHE.

3. Results and Discussions

3.1 Structural and XPS characterisation of the deposits on BDD

The SEM image of Fig. 1(a) illustrates the Cu₂O particles structure and morphology supported on the BDD substrate. The Cu₂O particles are cubic in shape and randomly deposited on the diamond surface. The electrochemical deposition of Cu₂O particles mostly occur at the electrochemically active sites with higher B concentration throughout the BDD surface as the substrate becomes more conductive with higher concentration of B dopant [51]. The elemental mapping of the Cu₂O cubic particles after NiO coating is shown in Fig. 1(b). The SEM image shows that NiO is deposited as nanoparticles onto the cubic shaped Cu₂O particles which are not fully covered with the NiO deposits. However, a layer of NiO nanoparticles is also seen on the underlying BDD surface. The fact that the NiO coating does not fully cover the whole surface of the Cu₂O particles was further verified through the XPS spectra (see Fig. 2(a-c)) which permits the co-catalyst effects of the NiO nanoparticles with the underlying surface of diamond to be assessed. Thick and overloading coverage of the Cu₂O cubic particles by NiO nanoparticles would result in a lower photocurrent response due to an increase in the distance that electron-hole pairs would need to travel to the reaction interface of the NiO-Cu₂O. Additionally, owing to a large band gap (~ 3.6 eV) of NiO [52], an increased loading content of NiO nanoparticles would hinder photo-absorption by the inner Cu₂O particles. TEM and HRTEM were used to characterise the microstructure and crystal structure of the NiO-Cu₂O particles in more detail. The TEM image in Fig. 1(c) shows

that Cu_2O is coated with NiO nanoparticles that form a thin shell on the surface of the Cu_2O . The size of the NiO nanoparticles are in the range of 3-6 nm as measured from the high magnification TEM image in the inset of Fig. 1(c). The crystal structures of the Cu_2O and NiO particles are well defined as revealed by the HRTEM image in Fig. 1(d), in which the corresponding lattice fringe spacings are clearly visible. The crystallographic inter-planar spacing 0.208 nm matched well with the (200) plane of NiO, which is in agreement with the XRD results shown in Fig. 2(d). The lattice fringe spacing of 0.24 nm denoted on the inset in Fig. 1(d) is related with the plane (111) of the Cu_2O cubic phase, which is the major crystal peaks observed in the XRD analysis (Fig. 2(d)).

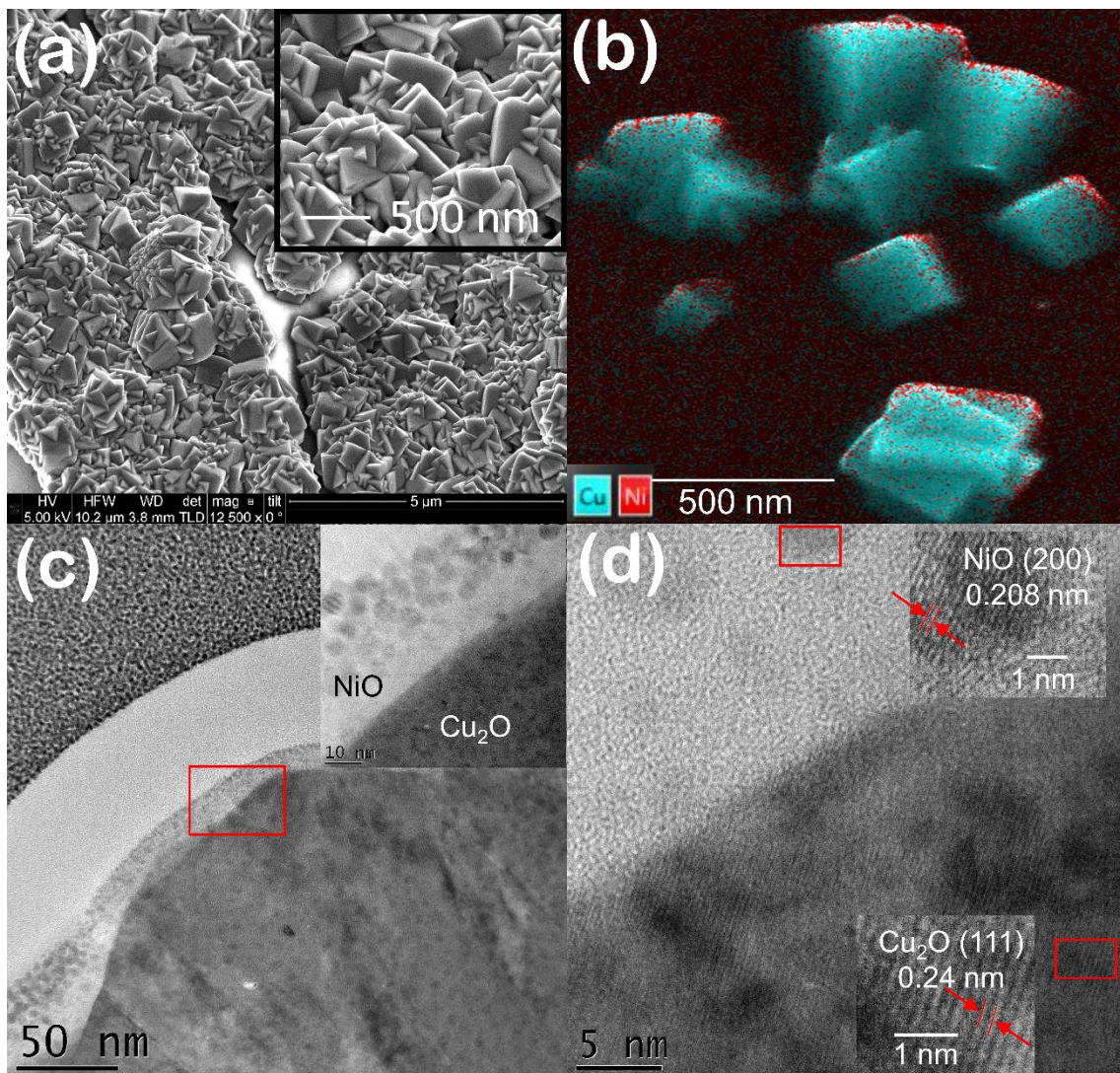


Fig. 1. (a) SEM images of the Cu_2O cubic particles (inset: high magnification image) and (b) elemental mapping of the NiO(15)- Cu_2O cubic particles on the BDD electrode, (c) cross-

section TEM image of the NiO(6)-Cu₂O (inset: high magnification image), and (d) HRTEM of the NiO(15)-Cu₂O/BDD and corresponding lattice spacing in the inset.

XPS spectra of the deposits on BDD are presented in Fig. 2. Fig. 2(a) shows the wide scan of the contaminant-free Cu₂O/BDD and indicates the presence of C 1s peak calibrated at 285 eV, O 1s peak and Cu 2p peak. The inset of Fig. 2(a) shows the Cu 2p peak of the Cu₂O deposit. For Cu (I) oxide, there is a main peak at 932.4 eV (Cu 2p_{3/2}) and a secondary peak at 952.3 eV (Cu 2p_{1/2}), respectively. A very weak satellite appears at 943 eV which is attributed to Cu₂O particles. Fig. 2(b) illustrates the survey of the NiO- Cu₂O/BDD electrode. The inset of Fig. 2(b) represents the Ni 2p peak. The two binding energy peaks located at 853.9 and 871.5 eV were assigned to Ni 2p_{3/2} and Ni 2p_{1/2} of NiO of the NiO-Cu₂O/BDD, respectively, and two smaller fitting peaks at 859.6 and 878 eV were assigned to NiO. A comparison of Cu 2p peaks of the Cu₂O and NiO-Cu₂O modified BDD is shown in Fig. 2(c). The main photoelectron peaks of Cu₂O of the Cu₂O/BDD electrode were obtained at 932.4 and 952.3 eV, respectively. There is a very weak satellite peak which is broader according to the literature [53] and differentiates it from the Cu metal. The second spectrum of the NiO-Cu₂O/BDD electrode in Fig. 2(c) shows the two main peaks of Cu 2p peak at a positive shifted binding energy by comparison with its counterpart at 934.7 and 954.6 eV, respectively. The presence of two extra satellite peaks at relatively higher binding energies, 942.9 and 962.4 eV, also indicate the potential existence of CuO on the surface. The latter is likely to arise due to the thermal treatment and therefore, oxidation of the catalysts at 200 °C for 3 hours. The positive binding energy shift of the Cu 2p peaks indicates that some electronic coupling of the core level of Ni 2p with the core level of Cu 2p has occurred, which is probably because Cu in the oxide state on BDD support has less electronegativity compared to Ni oxide which increases the electron cloud density of Ni. Such electronic interaction at the interface of the Cu₂O and NiO generates a synergistic effect, which can play a crucial role in the overall photocatalytic performance of NiO-Cu₂O/BDD photocathodes as we will see in the next section. Fig. 2(d) shows XRD patterns of the as prepared Cu₂O/BDD and after fifteen cycles of Ni⁺² ion precursor adsorption on Cu₂O/BDD and annealing at 200°C for 3 hours. The diffraction peaks observed at 2θ values of 36.5°, 42.4° and 61.5° correspond respectively to the lattice planes of (111), (200) and (220) of the cubic Cu₂O (JCPDS No. 05-0667). After annealing, a high diffraction intensity peak appeared at a value of 43.3°, which is attributed to the lattice plane (200) of the highly crystalline cubic structured NiO.

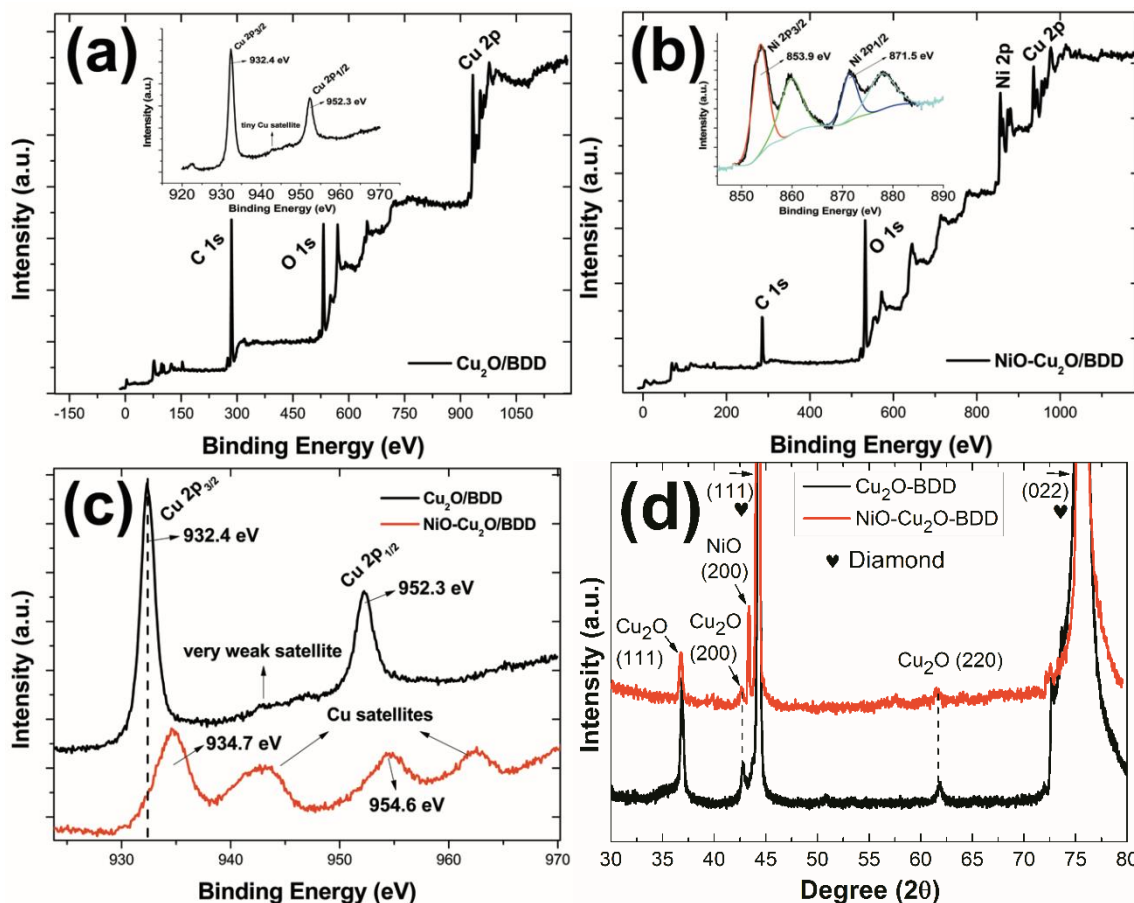


Fig. 2. (a) XPS spectrum of the $\text{Cu}_2\text{O}/\text{BDD}$ (inset: typical Cu 2p peak), (b) XPS spectrum of wide scan of the $\text{NiO-Cu}_2\text{O}/\text{BDD}$ (inset: typical Ni 2p peak), and (c) Comparison between the Cu 2p peaks of the Cu_2O and $\text{NiO-Cu}_2\text{O}$ modified BDD. (d) XRD patterns of the $\text{Cu}_2\text{O}/\text{BDD}$ and $\text{NiO(15)-Cu}_2\text{O}/\text{BDD}$.

3.2 Photoelectrochemical measurements of different photocathodes

The PEC performance of the photocatalysts was characterised by LSV under 0.2 Hz chopped light illumination with an intensity of $100 \text{ mW}/\text{cm}^2$ at a scan rate of $10 \text{ mV}/\text{s}$ in aqueous $0.1 \text{ M Na}_2\text{SO}_4$ electrolyte buffered at pH 6.5. Fig. 3 shows the photocurrent-potential curves of a series of photocathodes. The potential sweep started from 0.6 V and finished at -0.05 V .

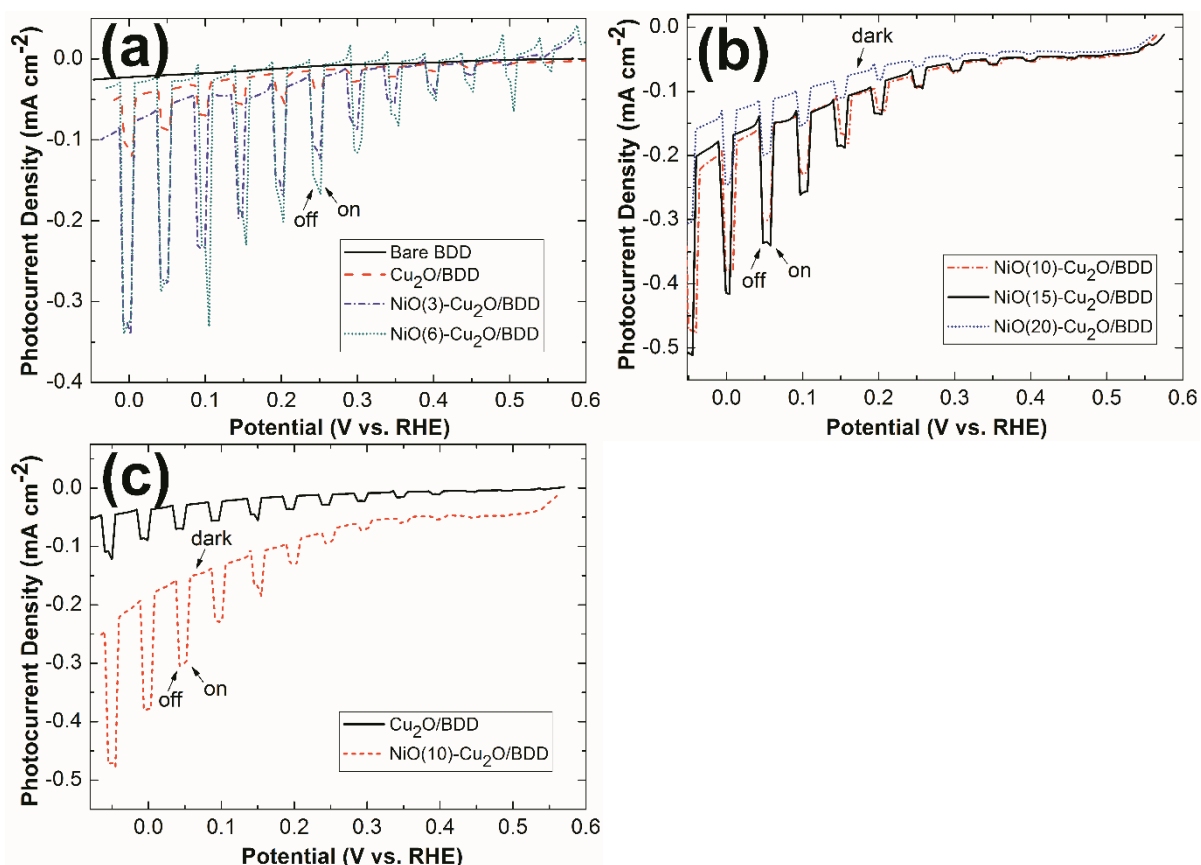


Fig. 3. Photoelectrochemical responses of different electrodes (a) bare BDD, Cu_2O , $\text{NiO}(3)\text{-Cu}_2\text{O}$ and $\text{NiO}(6)\text{-Cu}_2\text{O}$ modified BDD, (b) $\text{NiO}(10)\text{-Cu}_2\text{O}$, $\text{NiO}(15)\text{-Cu}_2\text{O}$ and $\text{NiO}(20)\text{-Cu}_2\text{O}$ modified BDD, and (c) $\text{Cu}_2\text{O}/\text{BDD}$ and $\text{NiO}(10)\text{-Cu}_2\text{O}$ modified BDD, respectively.

Fig. 3(a) illustrates the comparison of the photoelectrochemical response of bare BDD versus uncoated $\text{Cu}_2\text{O}/\text{BDD}$ and the NiO coated electrodes. For the sake of simplicity, parentheses are referring to the number of NiO coatings. There is no photoelectrochemical response for the unmodified BDD whereas there is a photocurrent response for the Cu_2O modified BDD. The phenomenon proved that Cu_2O shows a small catalytic activity towards hydrogen evolution reaction while absorbing light as a semiconductor material. The current started to increase gradually for $\text{Cu}_2\text{O}/\text{BDD}$ electrode and reached a maximum of $-0.12 \text{ mA}/\text{cm}^2$ at 0.0 V . The same behaviour is seen for the $\text{NiO}(3)\text{-Cu}_2\text{O}/\text{BDD}$ and $\text{NiO}(6)\text{-Cu}_2\text{O}/\text{BDD}$ electrodes but with higher photoelectrochemical activities. The photocurrent density of $-0.33 \text{ mA}/\text{cm}^2$ is obtained at 0.0 V for the NiO modified BDD electrodes with three and six coatings, respectively. The photocurrents increased slowly for low applied potential between 0.0 V and 0.3 V and increased rapidly after 0.25 V . In order to optimise the photocathode more NiO coatings were deposited and their PEC activities of are seen in Fig. 3(b). The photocurrent density of the $\text{NiO}(10)\text{-Cu}_2\text{O}/\text{BDD}$ and $\text{NiO}(15)\text{-Cu}_2\text{O}/\text{BDD}$ is and -

0.39 mA/cm² and -0.42 mA/cm² respectively, as acquired at 0.0 V, which is obviously higher than all the other photocathode electrodes. When the numbers of coating were increased further, the current decreased drastically. The photocurrent of the NiO(20)-Cu₂O/ electrode decreased to about -0.25 mA/cm² when measured at 0.0 V. The latter is likely to arise from the fact that more dip coatings increases the NiO thickness at the outer surface of the Cu₂O cubic particles due to higher NiO nanoparticles loading content, which hinders the photo absorption since NiO with a large band gap (~ 3.6 eV) is not photoactive in the visible region [52]. Of note in the case of more than 6 coatings is that the dark current is increased due to non-photocatalytic reactions of NiO such as capacitance charge storage. Fig. 3(c) compares the PEC performances of the NiO(10)-Cu₂O/BDD and Cu₂O/BDD electrodes. Clearly, as we showed previously the unmodified diamond gives no photoelectrochemical response in contrast with the Cu₂O particles modified diamond electrode. Thus, the photoelectrochemical response of the Cu₂O and NiO-Cu₂O modified BDD electrodes can be attributed to the visible light absorption by Cu₂O alone. The decoration of Cu₂O cubic particles by the NiO(10) nanoparticles enhances the photocurrent by ~ 2 to 4 times at potentials beyond 0.15 V (see Fig. 3(c)) after subtraction the dark current. The enhancement in the PEC activity is due to the fact that the band edge potential of Cu₂O coated with NiO makes a suitable band energy offset, which facilitates the fast transfer of the photogenerated electrons to the reaction interface and therefore, retards the undesired recombination losses of electron and hole pairs. Fig. 4 compares the photocurrent density versus applied potential of each electrode with the number of NiO coating cycles, which were measured in a two electrode configuration in the dark and under one sun illumination. PEC water splitting features of the two electrode system are similar to that of the LSV curves measured in three electrode system shown in Fig. 3. We can extract from the figure that photocurrent response initially increases with the dip coating up to 15 cycles and then decreases again with continuing NiO coating meaning that further coverage is unnecessary. However, higher loading content of NiO nanoparticles could increase the stability of the electrode but at a lower photocurrent response as we will see in the amperometric photostability section.

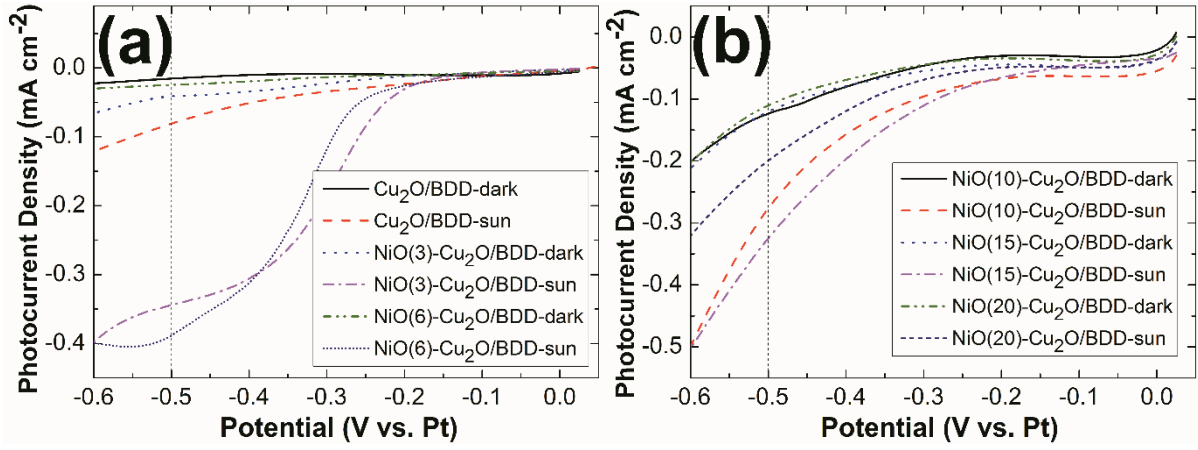


Fig. 4. Linear sweep voltammetry of (a) Cu₂O/BDD, NiO(3)-Cu₂O/BDD and NiO(6)-Cu₂O/BDD, and (b) NiO(10)-Cu₂O/BDD, NiO(15)-Cu₂O/BDD and NiO(20)-Cu₂O/BDD in two electrode system under 1 sun AM 1.5 illumination (100 mW/cm²).

The photoconversion efficiency (η) of light to hydrogen energy in terms of photocurrent density *versus* applied potential of (i) Cu₂O/BDD, (ii) NiO(3)-Cu₂O/BDD, (iii) NiO(6)-Cu₂O/BDD, (iv) NiO(10)-Cu₂O/BDD, (v) NiO(15)-Cu₂O/BDD, and (vi) NiO(20)-Cu₂O/BDD was measured under one sun illumination and is calculated using the following equation [54,55]:

$$\eta (\%) = \left[\frac{|J_{ph}| (mA cm^{-1}) \times (1.23 - |V_b|) (V)}{P_{total} (mW cm^{-2})} \right] \quad (1)$$

where J_{ph} is the photocurrent density obtained under an applied potential V_b between the working and the counter electrode, 1.23V is the standard water splitting reaction potential and P_{total} is the incident light intensity (100 mW cm⁻²). The PEC activity of the bare Cu₂O/BDD and NiO(6)-Cu₂O/BDD was negligible under dark condition (see Fig. 4(a)) and increases with more than 6 coating (see Fig. 4(b)) in the potential scan from 0.05 V to -0.6 V vs. Pt counter electrode. To quantitatively measure the photoconversion efficiency, dark current - 0.04 mA/cm² (see Fig. 4(a)) and -0.125 mA/cm² (see Fig. 4(b)) measured at -0.5 V vs. Pt, which was due to the non-photocatalytic reactions of NiO, were subtracted from the photocurrent for each electrode, respectively. As it was expected, the minimum conversion efficiency of 0.06% was obtained for the Cu₂O/BDD. In contrast, a maximum conversion efficiency of 0.26% and 0.28 % was obtained for the NiO(3)-Cu₂O/BDD and NiO(6)-Cu₂O/BDD electrodes, respectively. Likewise, the electrodes with ten and fifteen NiO coatings revealed 0.11% and 0.15% efficiencies, respectively (see Fig. 4(b)). The

photoconversion efficiency obtained for the NiO(20)-Cu₂O/BDD was only 0.05%. From the efficiencies we can see that the optimised NiO coating enhances the photoelectrons transfer to the reaction sites for the hydrogen evolution reaction, which becomes sluggish at increased surface coverage of Cu₂O by NiO since the photoelectrons have to travel further to reach the reaction interface before they recombine with holes.

3.3 Amperometric photostability of different photocathodes

Fig. 5 shows chronoamperometric features related to the photocatalytic stability of different photocathodes under 0.2Hz chopped light illumination at 0.05 V. Fig. 5(a) exhibits the Cu₂O/BDD electrode without NiO coating. As seen in the figure the uncoated Cu₂O/BDD photoelectrode is quite stable having a dark current about -0.01 mA/cm² and photocurrent increased under chopped illumination before it stabilised at -0.07 mA/cm². The NiO(10)-Cu₂O/BDD showed a photocurrent density of -0.3 mA/cm² for the first few seconds, which slightly decreased for a period of 30 minutes to -0.18 mA/cm² i.e., 60% of the initial photocurrent retained in Fig. 5(b). A less photocurrent drop is shown in Fig. 5(c) of NiO(15)-Cu₂O/BDD electrode where both dark and illumination photocurrent responses diminished significantly and stabilised with 70% of this photocurrent remaining after 30 minutes. There is a small photocurrent drop for the NiO(20)-Cu₂O/BDD electrode as shown in Fig. 5(d), in which it decreases from -0.15 mA/cm² to -0.13 mA/cm² for the first few seconds after which it is stabilised reaching -0.11 mA/cm² at 30 minutes. The dark current is close to zero in the chronoamperogram of Fig. 5(d) and 73% of this current remains after an operational period of 30 minutes. The obtained result shows that Cu₂O/BDD electrode with ten and fifteen NiO coatings are stable photoelectrode. Overall, NiO coated photoelectrodes gave higher photocurrent responses and better stability than that of the Cu₂O alone. The latter confirms that the NiO nanoparticles as co-catalyst increased the overall photocurrent density and stability in comparison with Cu₂O alone, which acts as a trap site for photogenerated electrons and thus retards the electron-hole recombination losses.

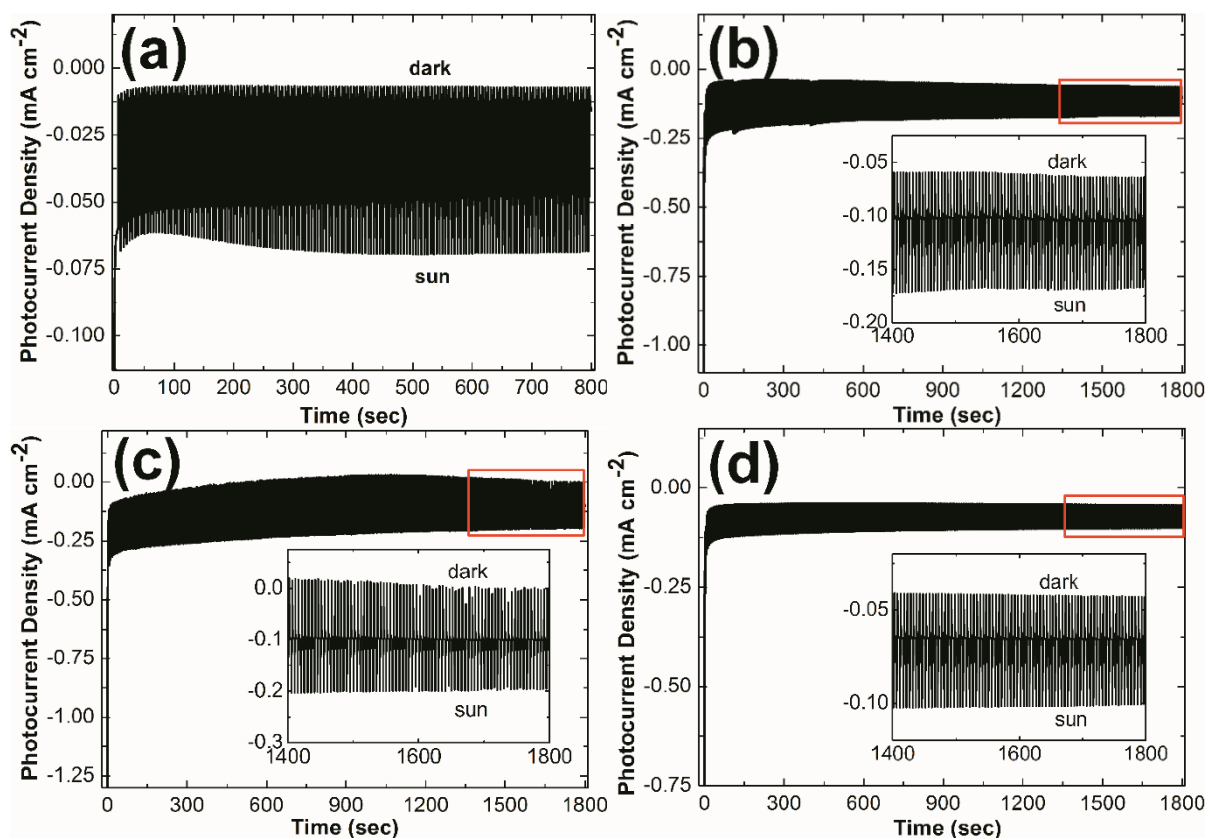


Fig. 5. Chronoamperograms of the photoelectrochemical response of the different photoelectrodes (a) $\text{Cu}_2\text{O}/\text{BDD}$, (b) $\text{NiO}(10)\text{-Cu}_2\text{O}/\text{BDD}$, (c) $\text{NiO}(15)\text{-Cu}_2\text{O}/\text{BDD}$ and (d) $\text{NiO}(20)\text{-Cu}_2\text{O}/\text{BDD}$ in an aqueous Na_2SO_4 electrolyte (0.1M, pH 6.5) under AM 1.5 chopped light illumination held at 0.05 V vs. RHE for 30 min (light on-off interval of 5s).

3.4 Electrochemical impedance

The electron transfer activity at the photocathode/solution interface was investigated through electrochemical impedance spectra (EIS) as shown in Fig. 6. The Nyquist plots of Fig. 6(a) were used to analyse the electrolyte interfacial charge transfer process at the NiO coated Cu_2O BDD electrodes. The measurements were carried out in the frequency range of 1 MHz to 0.1 Hz at the potential of 0.05 V under dark and light conditions. The semi-circular features of the Nyquist plots (Fig. 5(a)) at high frequencies define the charge transfer resistance [56]. As seen in Fig. 6(a) the semi-circular features of EIS measurements both in dark and under light illumination were observed suggesting that charge transfer resistance controls the kinetics across the electrode/electrolyte interface [57,58]. The arc radii of the $\text{Cu}_2\text{O}/\text{BDD}$ photoelectrode both under illumination and dark was higher which indicating a higher charge transfer resistance. However, arc radii of the NiO coated $\text{Cu}_2\text{O}/\text{BDD}$ photoelectrodes under illumination was much smaller than that of the dark. The latter is attributed to the increase of the electrode photoconductivity and the interfacial charge transfer

when they are irradiated by light. This phenomenon suggests that NiO nanoparticles on Cu₂O surface enhance the transfer of the photo-induced electrons to the reaction interface.

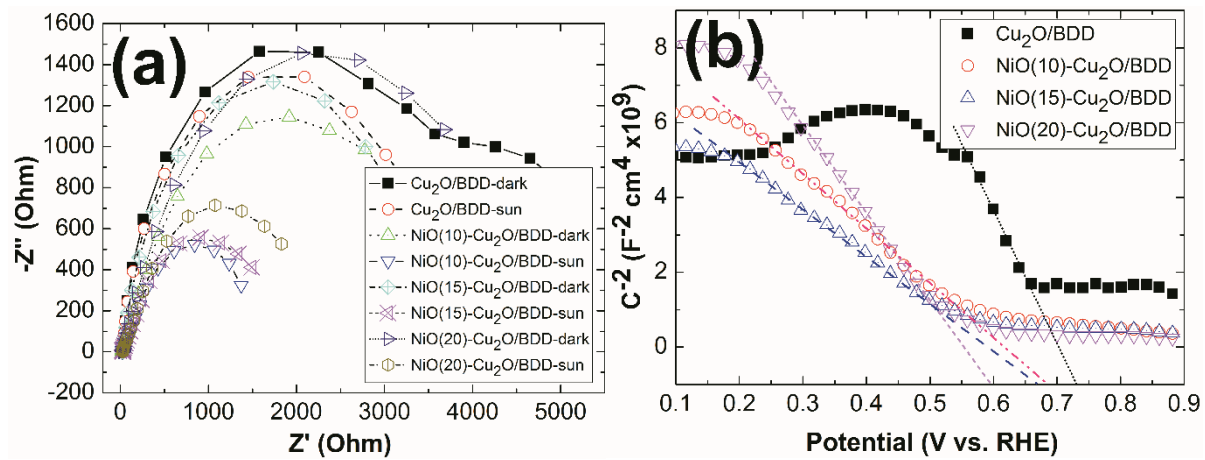


Fig. 6. (a) Nyquist plots of Cu₂O/BDD, NiO(10)-Cu₂O/BDD, NiO(15)-Cu₂O/BDD and NiO(20)-Cu₂O/BDD photoelectrodes in dark and under AM 1.5 light illumination in 0.1M Na₂SO₄ electrolyte buffered at pH 6.5 at 0.05 V vs. RHE (b) Mott-Schottky plots of NiO(10)-Cu₂O/BDD, NiO(15)-Cu₂O/BDD and NiO(20)-Cu₂O/BDD photoelectrodes in an aqueous Na₂SO₄ electrolyte (0.1M, pH 6.5) under dark.

Based on the interpretation of Alberly *et al.* of the Mott-Schottky plots [59] the capacitive behaviour of the semiconductor is associated with that of the Helmholtz layer in the electrolyte that provides the distribution of potential in the electrolyte as well as in the semiconductor for the accumulation, flat band transition and depletion. Therefore, for the capacitance measurements in the depletion region given that the potential is even across the Helmholtz layer, Mott-Schottky plots were used. The plot with $1/C^2$ vs. applied potential at a fixed frequency of 1 kHz was obtained according to the Mott-Schottky equation [60]:

$$\frac{1}{C^2} = \left(\frac{2}{e\epsilon\epsilon_0 N_A A^2} \right) \left[V - V_{fb} - \frac{k_B T}{e} \right] \quad (2)$$

where e is the electronic charge (1.602×10^{-19} C), ϵ is the relative permittivity ($\epsilon \sim 7.6$ for the Cu₂O) [54], ϵ_0 is the permittivity of vacuum (8.854×10^{-12} F/m), k_B is Boltzmann's constant (1.38×10^{-23} J/K), T is the absolute temperature (298 K), N_A is the carrier density, V_{fb} is the flatband potential, V is the applied potential and A is the area of the electrode. The active area of all electrodes was taken as the geometric surface area. From the linear fit of $1/C^2$ vs.

potential (V) in Fig. 6(b), V_{fb} for Cu_2O was measured using equation (3) [54] after a small correction for thermal contribution ($k_B T/e$) to the intercept (V_0) at zero on the potential axis.

$$V_{fb} = V_0 + k_B T/e \quad (3)$$

According to equation (3), V_{fb} were measured to be 0.75 V for $\text{Cu}_2\text{O}/\text{BDD}$, 0.71 V for $\text{NiO}(10)\text{-Cu}_2\text{O}/\text{BDD}$, 0.69 V for $\text{NiO}(15)\text{-Cu}_2\text{O}/\text{BDD}$ and 0.62 V for $\text{NiO}(20)\text{-Cu}_2\text{O}/\text{BDD}$ electrodes. The flatband potential, as indicated by the name, is the potential at which the Fermi energy level lies at the same energy as the electrolyte redox potential, and hence no charge transfer or band bending occurs at the semiconductor-liquid junction (SLJ) and thus, the conduction and valence bands are flat. The V_{fb} is considered to be a close approximation of the valence band (VB) edges of the p-type semiconductors [61] and therefore, the position of the conduction band (CB) edge can easily be calculated from the optical bandgap energies i.e. bandgap (eV) = valance band edge (eV) + conduction band edge (eV). The conduction bands are positioned at -1.42 V vs. RHE for $\text{Cu}_2\text{O}/\text{BDD}$, -1.46 V vs. RHE for $\text{NiO}(10)\text{-Cu}_2\text{O}/\text{BDD}$, -1.48 V vs. RHE for $\text{NiO}(15)\text{-Cu}_2\text{O}/\text{BDD}$ and -1.55 vs. RHE for $\text{NiO}(20)\text{-Cu}_2\text{O}/\text{BDD}$ electrodes. The CB edge position of our fabricated electrodes are more negative than that of the reported literature values [13,60], in which the higher CB edge position might have provided a larger electrochemical driving force for the hydrogen evolution reaction. The carrier density, N_A , was calculated from the slopes of the Mott-Schottky plots using the following equation [61]:

$$N_A = \frac{2}{e\epsilon\epsilon_0 S_{MS} A^2} \quad (4)$$

where e is the electronic charge, ϵ is the relative permittivity, ϵ_0 is the permittivity of vacuum, S_{MS} is the slope which can be obtained from the Mott-Schottky plot and A is the surface area of the electrode (1 cm^2). The slopes measured for each electrode are 14.2×10^9 for $\text{NiO}(10)\text{-Cu}_2\text{O}/\text{BDD}$, 11.7×10^9 for $\text{NiO}(15)\text{-Cu}_2\text{O}/\text{BDD}$ and 22.3×10^9 for $\text{NiO}(20)\text{-Cu}_2\text{O}/\text{BDD}$. Hence, the charge carrier density was found to be $1.32 \times 10^{21} \text{ cm}^{-3}$ for $\text{NiO}(10)\text{-Cu}_2\text{O}/\text{BDD}$, $1.60 \times 10^{21} \text{ cm}^{-3}$ for $\text{NiO}(15)\text{-Cu}_2\text{O}/\text{BDD}$ and $8.43 \times 10^{20} \text{ cm}^{-3}$ for $\text{NiO}(20)\text{-Cu}_2\text{O}/\text{BDD}$, respectively. The charge carrier density increases with the NiO nanoparticles content, which becomes the highest for $\text{NiO}(15)\text{-Cu}_2\text{O}/\text{BDD}$ electrode and decreases again with the continuation of loading of NiO e.g., $\text{NiO}(20)\text{-Cu}_2\text{O}/\text{BDD}$ electrode. The observed trend is similar to the

photocurrent responses, which implies that NiO nanoparticles on Cu₂O surfaces played a role in the suppression of electron-hole recombination, which became sluggish with the excessive coverage by NiO nanoparticles. We believe the overall trend is seen with an optimised surface coverage which decreases as a threshold in catalyst thickness is passed. The carrier densities in the fabricated NiO-Cu₂O particles were on the order of 10²¹ cm⁻³, which were much higher than those of the Cu₂O films fabricated by electrodeposition, namely 5×10¹⁷ cm⁻³ and 3.5×10²⁰ cm⁻³, as reported in the literature, respectively [62,63]. The higher charge carrier density suggests that NiO nanoparticles act as an acceptor and trap centre for the photogenerated electrons in the CB i.e. electron conduction mediator, which then transfer to the protons adsorbed on the surface of NiO for further reduction to hydrogen molecules. However, according to our measurement, the CB edge position of Cu₂O is -1.42 vs. RHE at pH 6.5, which increased up to -1.55 vs. RHE after coating with NiO nanoparticles (see Fig. 6(b)). The CB edge of the Cu₂O is lower than that of the NiO (-2.16 vs. RHE at pH 6) [52], which resists the transfer of the photogenerated electrons from the CB band of Cu₂O to the CB of NiO. It has previously been reported that NiO coating on Cu₂O nanowires was partially converted to Ni(OH)₂ under illumination and finally, photoreduced to Ni⁰ as the photogenerated electrons directly transferred from Cu₂O to Ni(OH)₂ [32]. To confirm the generation and reduction of Ni⁺²/Ni⁰ at the interface of Cu₂O/NiO during photocatalytic reaction, XPS measurement was carried out as shown in Fig. 7. After PEC reaction, two binding energy peaks located at 854.3 and 871.9 eV were assigned to Ni 2p_{3/2} and Ni 2p_{1/2} of NiO, respectively. A small positive shift in the binding energy indicates the possible change in the electronic state of the core level of Ni 2p orbitals [32]. A very small peak appeared at 849.9 eV was assigned to the 2p_{3/2} of Ni metal [43], which suggested the presence of metallic nickel on the catalyst surface during PEC reaction.

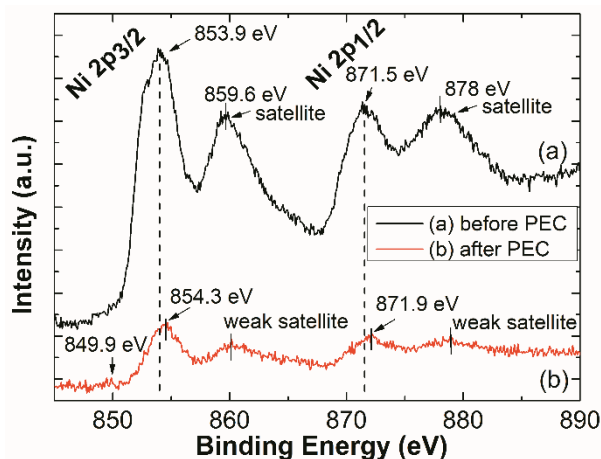


Fig. 7. XPS spectrum of Ni 2p peak of the NiO-Cu₂O/BDD sample before (a) and after photoelectrochemical test.

The experimental evidence suggest that under illumination, the VB electrons of Cu₂O were excited to the CB that provides an electron rich environment for the conversion of NiO to Ni(OH)₂ by the adsorbed aqueous protons on their surface. This conversion process was further catalysed by a higher electron cloud density localised on Ni⁺² due to the synergistic effect of the electron coupling as confirmed by XPS (see section 3.1). While the photogenerated holes in the VB were transferred to the electrolyte to oxidise water at the anode, photogenerated electrons in the CB were directly transferred to the Ni(OH)₂ and reduced Ni⁺² to metallic Ni⁰. The metallic Ni cluster acts as the electron sink to catalyse the H₂ evolution reaction. Ni(OH)₂ regenerates due to the increase in local pH at the reaction interface since protons are driven out as H₂ molecules thereby continuing the photocatalytic process. The PEC water splitting mechanism is shown in the schematic, Fig. 8. The deposition of small amount of NiO as nanoparticles on the surface of Cu₂O facilitates the fast transfer of photogenerated electrons from the p-type semiconductor (Cu₂O) to the Ni⁺²/Ni⁰/electrolyte interface to catalyse the H₂ evolution reaction.

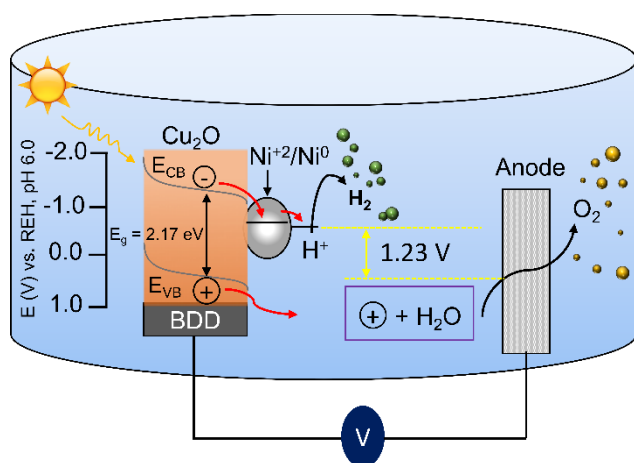


Fig. 8. Photoelectrochemical water splitting process on NiO nanoparticles decorated Cu₂O photocatalyst electrodeposited on BDD substrate.

4. Conclusions

In summary, a novel and low-cost photocathode material has been fabricated by an electrochemical method. The method involved the electrodeposition of Cu₂O particles on BDD electrodes from a surfactant free electrolyte followed by NiO coating. SEM data

revealed that the Cu₂O particles are cubic and NiO is well dispersed as nanoparticles on the Cu₂O and the unoccupied surrounding area of the BDD substrate. The semiconductor/co-catalyst (Cu₂O-NiO) presented higher photoelectrochemical activity in relation to the unmodified Cu₂O/BDD alone. The best photocurrent densities obtained at 0.0 V vs. RHE for the NiO(15)-Cu₂O/BDD and Cu₂O/BDD electrode were -0.42 mA/cm² and -0.12 mA/cm², respectively. Stability tests showed that the NiO nanoparticles loading is a crucial parameter in this regard. In our experiments the Cu₂O/BDD decorated with between 10 and 20 coating cycles of NiO nanoparticles are the most stable photocatalysts with optimised photocurrent responses and photoconversion efficiency. The photoconversion efficiency for NiO(6)-Cu₂O/BDD and NiO(15)-Cu₂O/BDD electrodes were measured to be 0.28% and 0.15% under an applied potential of -0.5 V compared to 0.06% for the unmodified Cu₂O/BDD electrode. Chronoamperometric responses showed a steady state current over a period of 30 minutes for NiO(15)-Cu₂O/BDD electrode with a photocurrent retention capacity of 70%. XPS data suggests electronic coupling of the core level of Ni 2p with the core level of Cu 2p at the interface between Cu₂O and NiO and therefore, synergistic effects leading to the enhanced charge separation and transfer to the reaction interface for hydrogen evolution. The charge carrier densities in the fabricated NiO-Cu₂O particles were on the order of 10²¹ cm⁻³, which is one order of magnitude higher than those of the literature values for Cu₂O films. This phenomena suggests that NiO nanoparticles act as an acceptor and trap centre for the photogenerated electrons in the conduction band and retards the recombination of photogenerated electrons and holes. Finally, EIS measurements for NiO-Cu₂O/BDD electrodes under illumination exhibited the higher charge transfer rates for the photo-induced electrons to the reaction interface. The Cu₂O modified electrodes with inexpensive co-catalyst of the current study have photoelectrochemical advantages which may be of benefit in their future use as a low cost option for solar hydrogen production.

Acknowledgment

Authors acknowledge Marie Curie Actions co-funded Irish Research Council Elevate fellowship ELEVATEPD/2014/15.

Notes

The authors declare no competing financial interest.

References

- [1] K. M. Parida, N. Biswal, D. P. Das, S. Martha, Visible light response photocatalytic water splitting over CdS-pillared zirconium-titanium phosphate (ZTP), *Int. J. Hydrogen Energy*, 35 (2010) 5262–5269.
- [2] N. Biswal, D. P. Das, S. Martha, K. M. Parida, Efficient hydrogen production by composite photocatalyst CdS-ZnS/Zirconium-titanium phosphate (ZTP) under visible light illumination, *Int. J. Hydrogen Energy* 36 (2011) 13452–13460.
- [3] S. Martha, D. P. Das, N. Biswal, K. M. Parida, Facile synthesis of visible light responsive $V_2O_5/N,S-TiO_2$ composite photocatalyst: enhanced hydrogen production and phenol degradation, *J. Mater. Chem.*, 22 (2012) 10695-10703.
- [4] Y. K. Hsu, Y. G. Lin, Y. C. Chen, Polarity-dependent photoelectrochemical activity in ZnO nanostructures for solar water splitting, *Electrochem. Commun.*, 13 (2011) 1383–1386.
- [5] O. Khaselev, J. A. Turner, A monolithic photovoltaic-photoelectrochemical device for hydrogen production via water splitting, *Science*, 280 (2013) 425.
- [6] US Department of Energy, Alternative fuels data center, http://www.afdc.energy.gov/pdfs/hyd_economy_bossel_eliasson.pdf
- [7] M. G. Walter, E. L. Warren, J. R. McKone, S. W. Boettcher, Q. Mi, E. A. Santori, N. S. Lewis, Solar water splitting cells, *Chem. Rev.*, 110 (2010) 6446–6473.
- [8] J. A. Turner, A realizable renewable energy future, *Science*, 285 (1999) 687–689.
- [9] X. Chen, S. Shen, L. Guo, S. S. Mao, Semiconductor-based photocatalytic hydrogen generation, *Chem. Rev.*, 110 (2010) 6503–6570.
- [10] D. Barreca, G. Carraro, V. Gombac, A. Gasparotto, C. Maccato, P. Fornasiero, E. Tondello, Supported metal oxide nanosystems from hydrogen photogeneration: Quo vadis?, *Adv. Funct. Mater.*, 21 (2011) 2611–2623.
- [11] M. Conte, A. Iacobazzi, M. Ronchetti, R. Vellon, Hydrogen economy for a sustainable development: state-of-the-art and technological perspectives, *J. Power Sources*, 100 (2001) 171–187.
- [12] N. A. Kelly, T. L. Gibson, Design and characterisation of a robust photoelectrochemical device to generate hydrogen using solar water splitting, *Int. J. Hydrogen Energy*, 31 (2006) 1658–1673.
- [13] A. Paracchino, N. Mathews, T. Hisatomi, M. Stefiak, S. D. Tilley, M. Grätzel, Ultrathin films on copper(I) oxide water splitting photocathodes: a study on performance and

- stability, *Energy Environ. Sci.*, 5 (2012) 8673-8681.
- [14] S. Somasundaram, C. Raman Nair Chenthamarakshan, N. R. de Tacconi, K. Rajeshwar, Photocatalytic production of hydrogen from electrodeposited p-Cu₂O film and sacrificial electron donors, *Int. J. Hydrogen Energy*, 32 (2007) 4661–4669.
 - [15] J. N. Nian, C. C. Hu, H. Teng, Elucidating the conductivity-type transition mechanism of p-type Cu₂O films from electrodeposition, *Int. J. Hydrogen Energy*, 33 (2008) 2897–2903.
 - [16] M. A. Mahmoud, W. Qian, M. A. El-Sayed, Following charge separation on the nanoscale in Cu₂O-Au nanoframe hollow nanoparticles, *Nano Lett.*, 11 (2011) 3285–3289.
 - [17] D. Barreca, P. Fornasiero, A. Gasparotto, V. Gombac, C. Maccato, T. Montini, E. Tondello, The potential of supported Cu₂O and CuO nanosystems in photocatalytic H₂ production, *ChemSusChem*, 2 (2009) 230–233.
 - [18] A. Paracchino, V. Laporte, K. Sivula, M. Grätzel, E. Thimsen, Highly active oxide photocathode for photoelectrochemical water reduction, *Nat. Mater.*, 10 (2011) 456–461.
 - [19] A. Radi, D. Pradhan D, Y. Sohn, K. T. Leung, Cu-Cu₂O core-shell nanoparticles on Si(100) by one-step, templateless, capping-agent-free electrodeposition, *ACS Nano*, 4 (2010) 1553–1560.
 - [20] H. Gerische, On the stability of semiconductor electrodes against photodecomposition, *J. Electroanal. Chem. Interfacial Electrochem.*, 82 (1977) 133–143.
 - [21] S. Deki, T. Yano, M. Mizuhata, A. Kajinami, Preparation and characterisation of copper(I) oxide nanoparticles dispersed in a polymer matrix, *J. Mater. Chem.*, 8 (1998) 1865–1868.
 - [22] W. M. Jin, J. H. Kang, J. H. Moon, Fabrication of 3D copper oxide structure by holographic lithography for photoelectrochemical electrodes, *ACS Appl. Mater. Interfaces*, 2 (2010) 2982–2986.
 - [23] K. H. Yoon, W. J. Choi, D. H. Kang, Photoelectrochemical properties of copper oxide films coated on an n-Si substrate, *Thin Solid Films*, 372 (2000) 250–256.
 - [24] M. F. Al-Kuhaili, Characterisation of copper oxide films deposited by thermal evaporation of cuprous oxide (Cu₂O), *Vacuum*, 82 (2008) 623–629.
 - [25] X. M. Liu, Y. C. Zhou, Electrochemical deposition and characterisation of Cu₂O nanowires, *Appl. Phys. A Mater. Sci. Process*, 81 (2005) 685–689.
 - [26] L. Chen, S. Shet, H. Tang, H. Wang, T. Deutsch, Y. Yan, J. Turner, M. Al-Jassim,

- Electrochemical deposition of copper oxide nanowires for photoelectrochemical applications, *J. Mater. Chem.*, 20 (2010) 6962–6967.
- [27] D. P. Singh, N. R. Neti, A. S. Sinha, O. N. Srivastava, Growth of different nanostructures of Cu₂O (nanothreads, nanowires and nanocubes) by simple electrolysis based oxidation of copper, *J. Phys. Chem. C*, 111 (2007) 1638–1645.
- [28] M. Le, M. Ren, Z. Zhang, P. T. Sprunger, R. L. Kurtz, J. C. Flake, Electrochemical reduction of CO₂ to CH₃OH at copper oxide surfaces, *J. Electrochem. Soc.*, 158 (2011) E45-E49.
- [29] O. Messaoudi, I. Ben assaker, M. Gannouni, A. Souissi, H. Makhlouf, A. Bardaoui, R. Chtourou, Structural, morphological and electrical characteristics of electrodeposited Cu₂O: Effect of deposition time, *Appl. Surf. Sci.*, 366 (2016) 383-388.
- [30] L. Yang, M. Zhang, K. Zhu, J. Lv, G. He, Z. Sun, Electrodeposition of flake-like Cu₂O on vertically aligned two-dimensional TiO₂ nanosheet array films for enhanced photoelectrochemical properties, *Appl. Surf. Sci.*, 391 (2017) 353-359.
- [31] K. Sun, X. Pang, S. Shen, X. Qian, J. S. Cheung, D. Wang, Metal oxide composite enabled nanotextured Si photoanode for efficient solar driven water oxidation, *Nano Lett.*, 13 (2013) 2064–2072.
- [32] C. Y. Lin, Y. H. Lai, D. Mersch, E. Reisner, Cu₂O/NiO_x nanocomposite as an inexpensive photocathode in photoelectrochemical water splitting, *Chem. Sci.*, 3 (2012) 3482-3487.
- [33] J. Cui, U. J. Gibson, A simple two-step electrodeposition of Cu₂O/ZnO nanopillar solar cells, *J. Phys. Chem. C*, 114 (2010) 6408–6412.
- [34] S. Zhang, S. Zhang, F. Peng, H. Zhang, H. Liu, H. Zhao, Electrodeposition of polyhedral Cu₂O on TiO₂ nanotube arrays for enhancing visible light photocatalytic performance, *Electrochem. Commun.*, 13 (2011) 861–864.
- [35] W. Siripala, A. Ivanovskaya, T. F. Jaramillo, S. H. Baeck, E. W. McFarland, A Cu₂O/TiO₂ heterojunction thin film cathode for photoelectrocatalysis, *Sol. Energy Mater. Sol. Cells*, 77 (2003) 229–237.
- [36] W. Shi, X. Zhang, S. Li, B. Zhang, M. Wang, Y. Shen, Carbon coated Cu₂O nanowires for photo-electrochemical water splitting with enhanced activity, *Appl. Surf. Sci.*, 358 (2015) 404-411.
- [37] J. Ran, J. Yu, M. Jaroniec, Ni(OH)₂ modified CdS nanorods for highly efficient visible-light-driven photocatalytic H₂ generation, *Green Chem.*, 13 (2011) 2708-2713.
- [38] J. Yu, Y. Hai, B. Cheng, Enhanced photocatalytic H₂-production activity of TiO₂ by

- Ni(OH)₂ cluster modification, J. Phys. Chem. C, 115 (2011) 4953–4958.
- [39] R. Subbaraman, D. Tripkovic, D. Strmcnik, K. C. Chang, M. Uchimura, A. P. Paulikas, V. Stamenkovic, N. M. Markovic, Enhancing hydrogen evolution activity in water splitting by tailoring Li⁺-Ni(OH)₂-Pt interfaces, Science, 334 (2011) 1256–1260.
- [40] J. S. Jang, S. H. Choi, D. H. Kim, J. W. Jang, K. S. Lee, J. S. Lee, Enhanced photocatalytic hydrogen production from water-methanol solution by nickel intercalated into titanate nanotube, J. Phys. Chem. C, 113 (2009) 8990–8996.
- [41] N. K. Shrestha, M. Yang, Y. C. Nah, I. Paramasivam, P. Schmuki, Self-organized TiO₂ nanotubes: visible light activation by Ni oxide nanoparticle decoration, Electrochem. commun., 12 (2010) 254–257.
- [42] T. Sreethawong, Y. Suzuki, S. Yoshikawa, Photocatalytic evolution of hydrogen over mesoporous TiO₂ supported NiO photocatalyst prepared by single-step- sol-gel process with surfactant template, Int. J. Hydrogen Energy, 30 (2005) 1053–1062.
- [43] L. Li, B. Cheng, Y. Wang, J. Yu, Enhanced photocatalytic H₂-production activity of bicomponent NiO/TiO₂ composite nanofibers, J. Colloid. Interface Sci., 449 (2015) 115–121.
- [44] G. Naponiello, I. Venditti, V. Zardetto, D. Saccone, A. Di Carlo, I. Fratoddi, C. Barolo, D. Dini, Photoelectrochemical characterisation of squaraine-sensitized nickel oxide cathodes deposited *via* screen-printing for *p*-type dye-sensitized solar cells, Appl. Surf. Sci., 356 (2015) 911–920.
- [45] S. H. Kim, M. Ebaid, J. H. Kang, S. W. Ryu, Improved efficiency and stability of GaN photoanode in photoelectrochemical water splitting by NiO cocatalyst, Appl. Surf. Sci., 305 (2014) 638–641.
- [46] C. K. Mavrokefalos, G. W. Nelson, C. G. Poll, R. G. Compton, J. S. Foord, Electrochemical aspects of Pt-Cu and Cu modified boron-doped diamond, Phys. Status Solidi Appl. Mater. Sci., 212 (2015) 2559–2567.
- [47] I. Shpilevaya, W. Smirnov, S. Hirs, N. Yang, C. E. Nebel, J. S. Foord, Nanostructured diamond decorated with Pt particles: preparation and electrochemistry, RSC Adv., 4 (2014) 531–537.
- [48] J. Svanberg-Larsson, G. W. Nelson, S. Escobar Steinvall, B. F. Leo, E. Brooke, D. J. Payne, J. S. Foord, A comparison of explicitly-terminated diamond electrodes decorated with gold nanoparticles, Electroanalysis, 28 (2016) 88–95.
- [49] CasaXPS, Processing software for XPS, <http://www.casaxps.com/>
- [50] L. Ley, S. Kowalczyk, R. Pollak, D. A. Shirley, X-ray photoemission spectra of

- crystalline and amorphous Si and Ge valence bands, *Phys. Rev. Lett*, 29 (1972) 1088–1092.
- [51] R. F. Mamin, T. Inushima, High conductivity of synthetic diamond, *Synthetic Metals*, 121 (2001) 1219–1220.
- [52] M. C. Toroker, D. K. Kanan, N. Alidoust, L. Y. Isseroff, P. Liao, E. A. Carter, First principles scheme to evaluate band edge positions in potential transition metal oxide photocatalysts and photoelectrodes, *Phys. Chem. Chem. Phys.*, 13 (2011) 16644–16654.
- [53] Thermo Scientific XPS, <http://xpssimplified.com/elements/copper.php>
- [54] A. A. Dubale, C. J. Pan, A. G. Tamirat, H. M. Chen, W. N. Su, C. H. Chen, J. Rick, D. W. Ayele, B. A. Aragaw, J. F. Lee, Y. W. Yang, B. J. Hwang, Heterostructured Cu₂O/CuO decorated with nickel as a highly efficient photocathode for photoelectrochemical water reduction, *J. Mater. Chem. A*, 3 (2015) 12482-12499.
- [55] Z. Chen, T. F. Jaramillo, T. G. Deutsch, A. K. Shwarsstein, A. J. Forman, N. Gaillard, R. Garland, K. Takanabe, C. Heske, M. Sunkara, E. W. McFarland, K. Domen, E. L. Miller, J. A. Turner, H. N. Dinh, Accelerating materials development for photoelectrochemical hydrogen production: Standards for methods, definitions, and reporting protocols, *J. Mater. Res.*, 25 (2010) 3–16.
- [56] Z. Zhang, R. Dua, L. Zhang, H. Zhu, H. Zhang, P. Wang, Carbon-layer-protected cuprous oxide nanowire arrays for efficient water reduction, *ACS Nano*, 7 (2013) 1709–1717.
- [57] C. Yang, P. D. Tran, P. P. Boix, P. S. Bassi, N. Yantara, L. H. Wong, J. Barber, Engineering a Cu₂O/NiO/Cu₂MoS₄ hybrid photocathode for H₂ generation in water, *Nanoscale*, 6 (2014) 6506–6510.
- [58] A. G. Tamirat, W. N. Su, A. A. Dubale, H. M. Chen, B. J. Hwang, Photoelectrochemical water splitting at low applied potential using a NiOOH coated codoped (Sn, Zr) α -Fe₂O₃ photoanode, *J. Mater. Chem. A*, 3 (2015) 5949–5961.
- [59] W. J. Albery, G. J. O'Shea, A. L. Smith, Interpretation and use of Mott-Schottky plots as the semiconductor/electrolyte interface, *J. Chem. Soc. Faraday Trans.*, 92 (1996) 4083-4085.
- [60] C. Li, Y. Li, J. J. Delaunay, A novel method to synthesize highly photoactive Cu₂O microcrystalline films for use in photoelectrochemical cells, *ACS Appl. Mater. Interfaces*, 6 (2014) 480-486.
- [61] J. N. Nian, C. C. Tsai, P. C. Lin, H. Teng, Elucidating the conductivity-type transition

- mechanism of p-type Cu_2O films from electrodeposition, J. Electrochem. Soc. 156 (2009) H567-H573.
- [62] A. Paracchino, J. C. Brauer, J. E. Moser, E. Thimsen, M. Graetzel, Synthesis and characterization of high-photocativity electrodeposited Cu_2O solar absorber by photoelectrochemistry and ultrafast spectroscopy, J. Phys. Chem. C, 116 (2012) 7341–7350.
- [63] K. Nakaoka, J. Ueyama, K. Ogura, Photoelectrochemical behavior of electrodeposited CuO and Cu_2O thin films on conducting substrates, J. Electrochem. Soc., 151 (2004) C661-C665.